Topological multiband photonic superlattices

Bikashkali Midya and Liang Feng

Topological multi-band photonic superlattices

Bikashkali Midya[*] and Liang Feng[†]

Department of Materials Science and Engineering,
University of Pennsylvania, Philadelphia, PA 19104, USA

A one-dimensional discrete lattice of dimers is known to possess topologically protected edge states when inter-dimer coupling is stronger than intra-dimer coupling. Here, we address richer topological properties of photonic superlattices having arbitrary number of elements in each unit cell. It is shown that the superlattice provides tunable number of topologically protected edge/interface states depending on certain restrictions on intra- and inter-dimer couplings maintaining inversion symmetry of the lattice. Simultaneous and stable propagation of multiple topological interface states, their interference pattern and stable oscillation are reported. As a practical application, the configuration can be used for topologically protected mode-division multiplexing through a narrow route in photonic devices.

Quest for new artificial materials and structures with non-trivial properties is at the heart of material science, optics and photonics research for continuously driving modern technology forward. The notion of topology and symmetry are most powerful tools in this endeavor. Both play a central role not only to understand elementary carrier particles and quasi-particles in natural systems, but also to tailor their properties in synthetic materials. In recent years, different topologically robust phases in various dimensions are discovered in electronic [1, 2], and engineered photonic [3, 4] systems. A conceptually simple one-dimensional (1D) topological system is the Su-Schrieffer-Heeger (SSH) model [5], initially introduced to explain charge transfer in polymer of acetylene molecules. This model features two distinct topological phases: a trivial phase characterized by a fully gapped energy spectrum, when inter-dimer coupling is less than intra-dimer coupling; and a non-trivial phase characterized by strongly localized zero-energy edge state lying within band gap, when couplings arrangement is reversed [6]. The most important feature, however, is that the edge state is topologically protected, being robust against various forms of disorder. In photonics and plasmonics, the SSH chain can be implemented with locally coupled cavities or waveguides with two alternating tunneling constants. Consequently, the topological zero mode in 1D has been theoretically investigated widely [7–20], and observed in recent experiments [21–27] with various systems either at the edge of an array or at the domain wall of two arrays with different dimerizations.

In this article, we theoretically address superlattices with complex unit cell structures and reveal the simultaneous existence of topologically protected multiple edge/interface states. Contrary to a lattice of dimers, which is always inversion symmetric and topological, a multi-partite lattice can be non-symmetric and non-topological. It is shown that the Zak phases of the corresponding Bloch bands are quantized provided the coupling coefficients are such that the superlattice is inversion symmetric; failing to which Zak phase takes arbitrary values [28, 29]. In a multi-band superlattice the topological properties of a particular band gap is determined by sum of the Zak phases (mod 2π) of all occupied bands below this gap [10, 30]. Based on analytical and numerical investigations on unit cells with different number of elements, we find that all the band gaps of a topological superlattice are non-trivial if inter-cell coupling is greater than some particular value at which the largest band gap in the system closes. In this case, robust localized edge states emerge inside all the topologically non-trivial gaps. Furthermore, the number of topological states are shown to be controlled by only tunning the inter-cell coupling parameter, when intra-cell couplings are kept unchanged. Because of the "particle-hole" symmetry of the system, topological edge states can be created (annihilated) in pairs for non-zero energies. Beam dynamics of multiple edge states, characterized by propagation constants residing in different band gaps, shows stable light propagation with breather like oscillation. Note that breathing oscillation of photonic Bloch waves—the Bloch oscillation—in a non-topological system was observed earlier in engineered waveguide array [31, 32]. Here we report similar oscillatory dynamics of non-Bloch states (i.e. localized edge states) in a topological waveguide array interface. The theoretical model, presented here, promises a practical application in topologically protected and robust mode-division multiplexing in photonic networks and devices through multiple orthogonal and robust edge-channels available in the system.

Multi-band superlattice. Consider a 1D discrete and periodic coupled system of $(M \times J)$ elements placed in M unit cells each composed of J components [Fig. 1(a)]. Corresponding Hamiltonian in the nearest-neighbor tight-binding approximation is given by

$$H = \sum_{m=1}^{M} \sum_{j=1}^{J-1} t_j a_{m,j}^{\dagger} a_{m,j+1} + \tau a_{m,J}^{\dagger} a_{m+1,1} + \text{h.c.} \quad (1)$$

where $a_{m,j}^{\dagger}$ $(a_{m,j})$ is the Bosonic creation (annihilation) operator at the j-th site in the m-th unit cell, t_j are the intra-cell tunneling amplitude from site j to adjacent site $j + 1$, and τ is the inter-cell tunneling amplitude. Here, t_j and τ are real and dimensionless, while

---

[*]Electronic address: bmidya@seas.upenn.edu
[†]Electronic address: fenglia@seas.upenn.edu

onsite potential is constant (assumed to be zero for simplicity). In photonics, the elements of a multipartite lattice can be considered as engineered waveguides or cavity resonators. However, a wide variety of other physical phenomena e.g. in ultracold bosons in optical lattice [33], sound propagation in acoustics network [34], qubit transfer in a quantum network [35] etc, can also be modeled by equation (1). For a given energy, β, the stationary solution of the system is sought in the form $|\psi(t,\beta)\rangle = e^{-i\beta t}\sum_{m,j} A_{m,j}\, a_{m,j}^\dagger|0\rangle$, where $|0\rangle$ is the vacuum with zero amplitude in all the sites. In order to obtain the site amplitudes $A_{m,j}$, we substitute the expression of $|\psi\rangle$ in the Schrödinger equation $i\frac{\partial|\psi\rangle}{\partial t} - H|\psi\rangle = 0$, and obtain the following set of equations written in a matrix form

$$\mathbf{HA} = \beta\mathbf{A}, \qquad (2)$$

where $\mathbf{A} = [A_1, A_2, ..., A_{MJ}]^T$ with $A_n \equiv A_{m,j} = \langle m,j|\psi(0,\beta)\rangle$ such that $n = (m-1)J + j$. $\mathbf{H}$ is a $(MJ \times MJ)$ tridiagonal matrix with diagonal elements are all zero and principal off-diagonals are formed by the band $(t_1, t_2, ..., t_{J-1}, \tau)$. The discrete spectrum, β, of a finite system can be obtained using the numerical diagonalization technique with an open boundary condition: $A_0 = A_{MJ+1} = 0$ i.e. energy exchange outside the lattice is not allowed. For $J = 1$ and 2, our model reduces to widely studied homogeneous lattice and topological Su-Schrieffer-Heeger lattice model, respectively. Of interest is the superlattice with $J > 2$ and coupling parameters which are symmetric with respect to the center of the unit cell. Surprisingly, in this case, the spectrum of the system appears in two distinct forms (as shown in figure 1(b-g) for particular examples): spectrum with (without) bound states inside all the $(J-1)$ energy gaps when the inter-cell coupling τ is greater (less) than some particular values depending on intra-cell couplings (details are described below). Furthermore, the states deep in the gap are found to be localized at the edges of the lattice (an example is shown in fig 2(e) for $J = 4$). The topological origin for the appearance of such edge modes is explained in the following.

Topological characterization. In order to better understand the topological properties of the superlattice, we perform Fourier transform on the creation and annihilation operators: $a_{m,j} = \sum_k e^{ikam}\tilde{a}_{k,j}/\sqrt{M}$, for all j and m. Here a is the lattice constant, and $\tilde{a}_{k,j}^\dagger(\tilde{a}_{k,j})$ is the plane wave creation (annihilation) operator with the crystal momentum $k \in [-\pi/a, \pi/a]$. The Hamiltonian in the reciprocal space, therefore, reduces to

$$\widetilde{H} = \sum_k \sum_{j=1}^{J-1} t_j\, \tilde{a}_{k,j}^\dagger\tilde{a}_{k,j+1} + \tau e^{ika}\, \tilde{a}_{k,J}^\dagger\tilde{a}_{k,1} + \text{h.c.} \qquad (3)$$

which can be cast into the convenient form $\widetilde{H} = \sum_k \mathcal{A}^T\mathcal{H}(k)\mathcal{A}$, where $\mathcal{A} = [\tilde{a}_{k,1}, ..., \tilde{a}_{k,J}]^T$; the kernel $\mathcal{H}$ represents the Bloch Hamiltonian of the system and a central object of investigation for topological properties
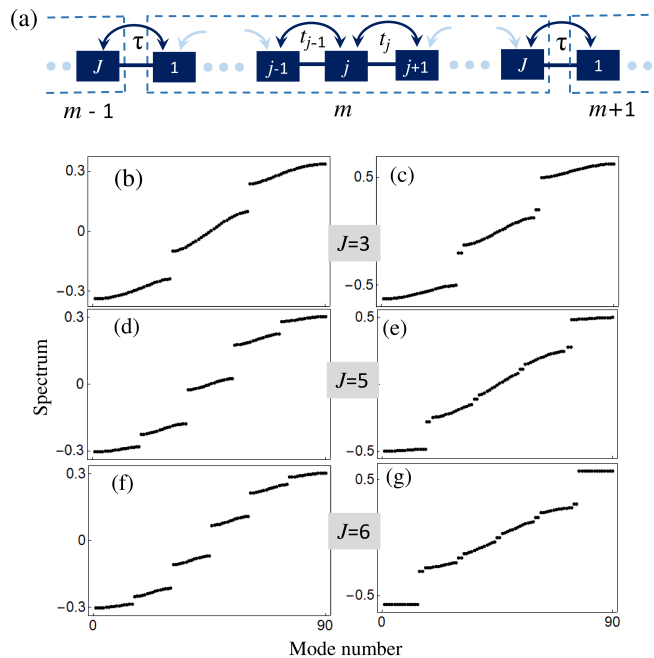

FIG. 1: (a) A schematic of a photonic superlattice with J elements in each unit cell. t_j and τ are intra-cell, and inter-cell couplings, respectively. Eigenspectrum, β, of superlattices with $J = 3, 5$ and 6 elements in a unit cell are shown in (b,c), (d,e) and (f,g), respectively. Emergence of bound states inside the energy gap are seen in (c,e,g). The parameters chosen are (b) $t_1 = t_2 = 0.2, \tau = 0.1$; (c) same as in (b) but $\tau = 0.5$; (d) $t_1 = t_4 = 0.2, t_2 = t_3 = 0.15, \tau = 0.05$, (e) same as in (d) but $\tau = 0.5$; (f) $t_1 = t_5 = 0.2, t_2 = t_3 = t_4 = 0.15, \tau = 0.05$; (g) same as in (f) but $\tau = 0.5$.

of the lattice. In this case, the band structure and corresponding normalized Bloch wave functions are given by $\mathcal{H}(k)|u_j(k)\rangle = \beta_j(k)|u_j(k)\rangle$. The topological properties of a band gap in a 1D system is characterized by the sum of Zak phases of all the isolated bands below the corresponding band gap [30, 36]:

$$\gamma = \sum_{j\in\text{occ.}} \gamma_j, \quad \gamma_j = i\int_{-\pi/a}^{\pi/a} dk\, \langle u_j(k)|\frac{d}{dk}|u_j(k)\rangle. \qquad (4)$$

Here, sum is considered over all occupied bands below a particular band gap, and γ_j (mod 2π) is the Zak phase of the isolated j-th band. The topological properties of a particular band gap is therefore not affected by the upper bands [10]. We have found that either 0 or π quantization of the Zak phase is possible only when the system possesses inversion symmetry; as first pointed out by Zak [28, 29], the relationship between quantization of γ_j and the quantization of the band center are intimately connected. When there is no such symmetry the values of γ_j is found not to quantize and takes arbitrary values [a numerical example is shown below in Fig. 2(g)].

In a generic case, it is straightforward to show that the Bloch Hamiltonian $\mathcal{H}$ is time-reversal symmetric, i.e., $T\mathcal{H}(k)T^{-1} = \mathcal{H}^*(-k) = \mathcal{H}(k)$, whenever all the coupling amplitudes are real. While it is inversion symmetric, i.e., $\Pi\mathcal{H}(k)\Pi^{-1} = \mathcal{H}(-k)$, provided that $t_j = t_{J-j}$
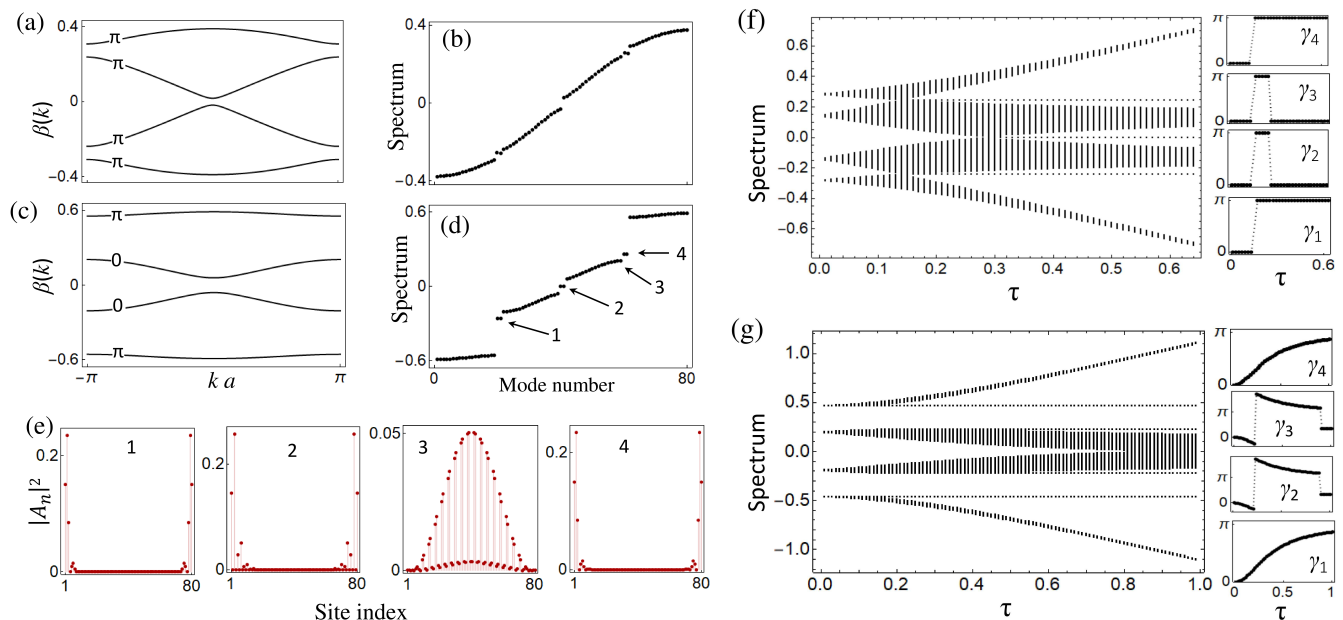
FIG. 2: Topological properties of a superlattice with four elements in a unit cell. (a) and (c) show the band structures together with corresponding Zak phases for a $t_1 t_2 t_1 \tau$ lattice with two different sets of parameters. The first and third gaps in (a), and all the gaps in (c) are topologically non-trivial. (b) and (d) show discrete spectra corresponding to the band structures of (a) and (c), respectively. These spectra show emergence of edge states inside respective topologically non-trivial gaps. In (e), mode intensities $|A_n|^2$, for the states indicated by arrows in (d), are shown. The states are exponentially localized in 1,2, and 4; whereas state at 3 is extended in bulk. The parameters chosen are $t_1 = 0.2, t_2 = 0.15$, for all the figures in (a$\cdots$e); while $\tau = 0.24$ in (a,b) and 0.5 in (c,d,e), respectively. (f) Shows the spectra of a topological superlattice when inter-cell coupling τ is tuned by keeping intra-cell couplings $t_{1/2}$ fixed. Note that, as mentioned in the text, first and third band gaps close when $\tau = t_2 = 0.15$, while middle gap closes when $\tau = t_1^2/t_2 = 0.27$. In this case, quantization of Zak phases is observed as shown [in the right-hand side panels of (f)] for all the bands. (g) Same as in (f) but for a non-topological ($t_1 t_2 t_3 \tau$) lattice with anisotropic coupling parameters ($t_1 = 0.3, t_2 = 0.1, t_3 = .45$) i.e. no inversion symmetry in the system. In this case, although, bound states inside gaps are visible, but they are not topological as corresponding Zak phases are not quantized. The band inversion, as a result of band gap closing and reopening, is not observed in (g).

for all j; here $\Pi = \sigma_x \otimes \sigma_x$ is the anti-diagonal matrix with non-zero entries as 1 and plays the role of an inversion operator [6]. Remarkably, all the band gaps in a system with inversion symmetry are found to be topologically non-trivial (trivial) i.e. sum of γ_j (mod 2π) for all bands below that gap is π (0) if $\tau > \tau_{max}(\{t_j\})$ ($\tau < \tau_{min}(\{t_j\})$). Here, τ_{max} and τ_{min} are the values of τ, depending on intra-cell coupling parameters $\{t_j\}$, for which the largest and smallest band gaps in the system disappears, respectively. In general, the values of $\tau_{max/min}$ can be evaluated numerically when J is large. However, in order to get analytical insight, below we elaborate our findings for a superlattice with four elements in a unit cell ($J = 4$).

For $J = 4$, the Bloch Hamiltonian is given by

$$\mathcal{H}(k) = \begin{bmatrix} 0 & t_1 & 0 & \tau e^{-ika} \\ t_1 & 0 & t_2 & 0 \\ 0 & t_2 & 0 & t_3 \\ \tau e^{ika} & 0 & t_3 & 0 \end{bmatrix}, \quad (5)$$

which satisfies inversion symmetry in the following two coupling schemes: $t_1 t_1 t_1 \tau$ and $t_1 t_2 t_1 \tau$. We consider the latter case for the following discussion. The dispersion

relation, in this case, is given by

$$\cos ka = f(\beta) = \frac{\beta^4 - (2t_1^2 + t_2^2 + \tau^2)\beta^2 + t_1^4 + t_2^2 \tau^2}{2t_1^2 t_2 \tau}, \quad (6)$$

which gives four energy bands, as shown in figure 2(a,c). The band edges are obtained (after solving $|f(\beta)| = 1$) as

$$\beta_1^\pm = [\pm t_2 - (T + \tau)]/2, \quad \beta_2^\pm = [t_2 \pm (T - \tau)]/2,$$
$$\beta_3^\pm = -\beta_2^\mp, \quad \beta_4^\pm = -\beta_1^\mp, \quad (7)$$

where $T = \sqrt{4t_1^2 + (t_2 - \tau)^2}$. Hence, the energy gaps $\Delta \beta = |\beta_j^+ - \beta_{j+1}^-|$ between j-th and $(j+1)$-th bands are given by

$$\Delta\beta_{12} = \Delta\beta_{34} = |t_2 - \tau|, \quad \Delta\beta_{23} = |t_2 + \tau - T|. \quad (8)$$

This shows that the first and third band gaps close when $\tau = t_2$, while second gap closes for $\tau = t_1^2/t_2$. In this case, we found two extreme cases: when $\tau > max(t_2, t_1^2/t_2)$, the Zak phases for the isolated band are $\gamma_1 = \gamma_4 = \pi$ and $\gamma_2 = \gamma_3 = 0$, implying that all the three band gaps are topologically non-trivial. While all the gaps are topologically trivial, when $\tau < min(t_2, t_1^2/t_2)$,

because in this case Zak phases for all the isolated bands are quantized to zero. For τ in the intermediate values between these two extreme cases, the number of topologically non-trivial band gaps is less than three. Hence, the number of topological states can be controlled by tunning the inter-cell coupling parameter when all other parameters are fixed. Particular examples of these findings are illustrated in Fig. 2(a-e) together with numerically evaluated spectrum and edge states; while the full spectrum versus a parameter sweep is shown in Fig. 2(f,g) for both a topological and a non-topological (i.e. without inversion symmetry) lattice. In the former case, the band inversion as a result of band gap closing and reopening is observed. This phenomena of band inversion is absent in the latter case. As shown in Fig. 2, the band structures (and spectra) appear to be mirror symmetric with respect zero energy i.e. $\beta(k) = -\beta(k)$, as a consequence of the particle-hole symmetry of the Hamiltonian: $\Sigma_y \mathcal{H} \Sigma_y^{-1} = -\mathcal{H}^*$, where $\Sigma_y = \sigma_x \otimes \sigma_y$ (the particle-hole symmetry relation holds provided $\mathcal{H}$ satisfies inversion-symmetry condition mentioned above). This symmetry also explains the simultaneous appearance of two edge states at the same edge for $\pm\beta$ with $\beta \neq 0$ [36]. Therefore, the edge states, in this case, can always be created/destroyed in pairs for non-zero energies in a superlattice with $J > 2$.

Based on similar analytical and numerical investigations for $J = 1, \cdots 8$, we conjecture here that above mentioned results hold in general cases. The examples shown earlier in Fig. 1(b,d,f) are, in fact, topologically trivial; whereas those shown in Fig. 1(c,e,g) are topologically non-trivial. Owing to the topology, two band gaps of different topological properties can not be adiabatically transformed one into other without creating a edge state inside the non-trivial gap. Consequently, topologically protected interface states can be induced in all the topologically non-trivial band gaps when two lattices of different topological properties are combined to form an interface (see Fig. 3 for examples).

Dynamics of interface states propagation. As an application of the theory we have simulated the dynamics of the interface states propagation in photonic array composed of waveguides evanescently coupled to each other. Light evolution in such a structure is governed by the coupled-mode equation which is equivalent to the Schrödinger equation mentioned above [37, 38]. The propgation distance z here plays the role of time in Schrödinger equations, and the spectral parameter β plays the role of a normalized propagation constant. The array supermode is described in terms of the individual waveguide mode amplitudes, and the details of the field between the waveguides is encoded into a single parameter—the coupling constant. Couplings between waveguides can be achieved when two waveguides are brought sufficiently close together that the evanescent fields overlap. By lithographic technique the separation between waveguides, and hence the coupling modulation, can be precisely controlled [27]. As shown schematically in Fig. 3(a), a topological interface can be created by combining two waveguide systems of different topolog-
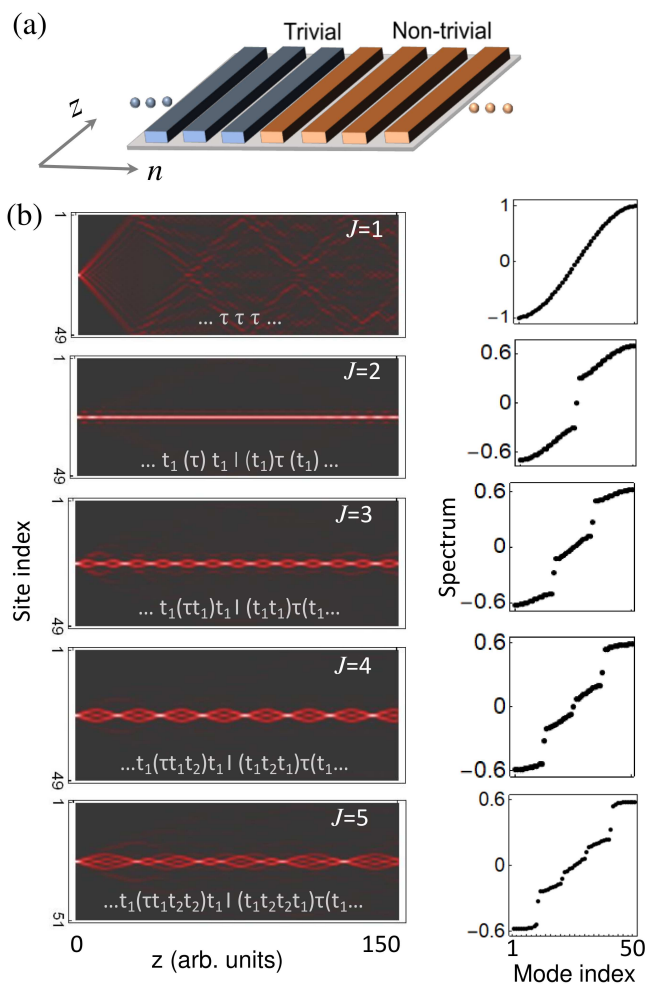

FIG. 3: (a) A schematic of two evanescently coupled waveguide superlattices of different topological band gap properties. In the left-hand side panels of (b), we have shown the light intensity evolution, $|A_n(z)|^2$, through the interfaces of such superlattices when each unit cell contains $J = 1, \cdots, 5$ elements, respectively. A single site at $n = 25$ is excited in all these cases. Corresponding propagation-constant spectra are shown at the right-hand side panels. Linear dispersion and propagation of one interface state are seen when $J = 1$ and 2, respectively. For $J = 3, 4$ and 5, stable propagation of 2, 3 and 4 interface states are seen. The particular coupling arrangements, used to create topological interfaces, are shown over the respective panels of intensity evolution; right- (left-) hand side represents topologically non-trivial (trivial) coupling schemes. The parameters for $J = 1, 2$ are $\tau = 0.5$ and $t_1 = 0.2$. For $J = 3, 5, 4$ we considered same set of parameters as in Fig. 1(c),(e) and 2(d), respectively.

ical properties [e.g., in the Fig. 3(a), waveguide array in the right (left) represents a topologically non-trivial (trivial) array]. Light propagation in such interfaces is simulated by directly integrating the coupled-mode equation: $i\dot{\mathbf{A}}(z) + \mathbf{H}\mathbf{A}(z) = 0$, with initial condition $A_n(0) = \delta_{nn'}$, i.e. light injection at the interface site n'. The solution have following succinct form

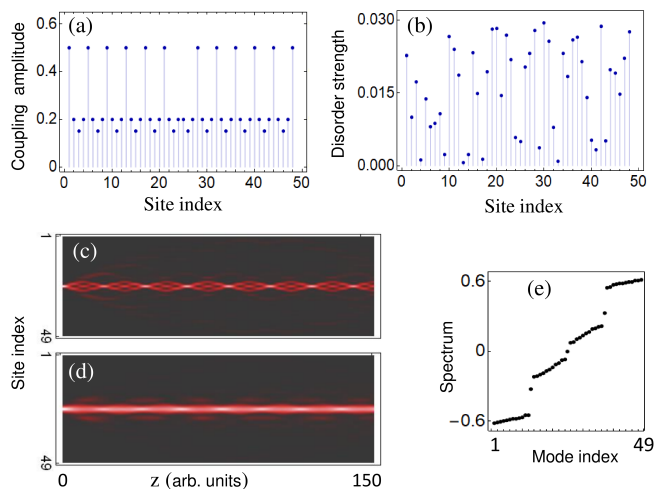$$A_n(z) = \sum_\ell \left[e^{i\mathbf{H}z}\right]_{n\ell} A_\ell(0). \tag{9}$$

FIG. 4: Robustness against disorder. (a) Shows the coupling amplitudes of an unperturbed waveguide lattice for which the beam dynamics was shown in Fig. 3(b) for $J = 4$. (c) and (d) shows the robust beam dynamics when random coupling disorder is added to the lattice; the disorder strengths are shown in (b). In (c) a single site at $n = 25$ is excited, while in (d) an initial Gaussian beam $A_n(z = 0) = e^{-(n-25)^2/3}$ is considered. (e) shows the propagation-constant spectrum for the lattice with added disorder.

Figure 3(b) shows the intensity evolutions, $|A_n|^2$, in the superlattices composed of $J = 1, 2, 3, 4$ and 5 elements. For $J = 1$, which is always topologically trivial, well known linear dispersion is observed. For $J = 2$ (corresponds to the widely studied SSH lattice) propagation of one interface mode is seen. On the other hand, for $J > 2$, stable interference pattern is seen, which is the signature of simultaneous propagation of multiple interface states corresponding to different propagation constants. The interface states form a breather like oscillation while propagating in space (similar phenomena are observed because of soliton-soliton interaction in non-linear optics [39]). Note that there is no nonlinearity present in the system under consideration; the formation of stable breathers is due to interference of topological linear modes of different propagation constants.

It is worth mentioning here that the oscillation of optical waves can also appear in non-topological and linear lattices—e.g., the Bloch oscillation—which was observed in engineered waveguide array with a linearly increasing

effective-index gradient across the array [31, 32]. However, in our case the stable oscillation can be observed with zero-refractive index modulation i.e. with waveguides having identical individual propagation constant. A single site excitation, in case of the Bloch oscillation, spread symmetrically over the whole array before refocusing into the initial guide. In contrast, in the topological array the energy of the excitation remains confined within few sites at the interface [as shown in the Fig. 3(b)]. This is because, in the later case, the states inside different band gaps are predominantly localized at the interface; while the excitation energy, in the former case, is distributed over the Bloch states residing in the entire bulk.

Finally, we have verified the stability, of interface states propagation, against moderate disorder in all the cases investigated in figure 3(b). In particular, the robustness against random disorder (of strength 0-15% of t_2) is illustrated in Fig. 4 for a superlattice with $J = 4$. Stable propagation is observed for both a single site excitation [Fig. 4(c)] and a Gaussian wave packet [Fig. 4(d)].

In summary, we have put forwarded an elegant approach to create tunable number of topologically protected edge/interface states in a superlattice consists of complex unit cell structures with suitably coupled elements respecting inversion symmetry. The coexistence of multiple topological states, their controllability (by manipulating coupling amplitudes), and stable propagation dynamics, addressed here, can be used for 'topological' mode division multiplexing for a single-wavelength carrier wave through a narrow route in photonic devices. The breather like oscillations reported here can be observed in realistic experiments on silicon-on-insulator waveguide platform by using ultrafast optical metrology. As a final note, despite its conceptual simplicity, the model can be used for a description of diverse 1D topological phenomena related to electronic, plasmonic, polaritonic, mechanical, and acoustic systems and can be generalized for energy non-conserving (i.e. non-Hermitian) systems.

[1] M.Z. Hasan, and C.L. Kane, Colloquium: topological insulators, Rev. Mod. Phys. **82**, 3045 (2010).
[2] X. Qi and S. Zhang, Topological insulators and superconductors, Rev. Mod. Phys. **83**, 1057 (2011).
[3] F. D. M. Haldane and S. Raghu, Possible Realization of Directional Optical Waveguides in Photonic Crystals with Broken Time-Reversal Symmetry, Phys. Rev. Lett. **100**, 013904 (2008).
[4] L. Lu, J. D. Joannopoulos and M. Soljacic, Topological photonics, Nature Photonics **8**, 821 (2014).
[5] W. P. Su, J. R. Schrieffer, and A. J. Heeger, Solitons in polyacetylene, Phys. Rev. Lett. **42**, 1698 (1979).
[6] J.K. Asbóth, L. Oroszlány, and A. Pályi, A Short Course on Topological Insulators, Lecture Notes in Physics 919 (2016).
[7] H. Schomerus, Topologically protected midgap states in complex photonic lattices, Opt. Lett. **38**, 1912 (2013).
[8] S. Longhi, Zak phase of photons in optical waveguide lattices, Opt. Lett. **38**, 3716 (2013).
[9] V. Dal Lago, M. Atala, and L. F. Torres, Floquet topo-

logical transitions in a driven one-dimensional topological insulator, Phys. Rev. A **92**, 023624 (2015).

[10] M. Xiao, Z.Q. Zhang, and C.T. Chan, Surface Impedance and Bulk Band Geometric Phases in One-Dimensional Systems, Phys. Rev. X **4**, 021017 (2014).

[11] L. Li, Z. Xu, and S. Chen, Topological phases of generalized Su-Schrieffer-Heeger models, Phys. Rev. B **89**, 085111 (2014).

[12] B. Qi, L. Zhang, and L. Ge, Defect States Emerging from a Non-Hermitian Flatband of Photonic Zero Modes, Phys. Rev. Lett. **120**, 093901 (2018).

[13] C. Yuce, Edge states at the interface of non-Hermitian systems, Phys. Rev. A **97**, 042118 (2018).

[14] L. Ge, Symmetry-protected zero-mode laser with a tunable spatial profile, Phys. Rev. A **95**, 023812 (2017).

[15] J. Arkinstall, M. H. Teimourpour, L. Feng, R. El-Ganainy, H. Schomerus, Topological tight-binding models from non-trivial square roots, Phys. Rev. B **95**, 165109 (2017).

[16] Q. Cheng, Y. Pan, Q. Wang, T. Li, and S. Zhu, Topologically protected interface mode in plasmonic waveguide arrays, Lasers & Photonics Rev. **9**, 392 (2015).

[17] C.W. Ling, M. Xiao, C. T. Chan, S. F. Yu, and K. H. Fung, Topological edge plasmon modes between diatomic chains of plasmonic nanoparticles, Optics Express **23**, 2021 (2015).

[18] Y. Hadad, V. Vitelli, and A. Alu, Solitons and Propagating Domain Walls in Topological Resonator Arrays, ACS Photonics, **4**, 1974 (2017).

[19] L. Jin, P. Wang and Z. Song, Su-Schrieffer-Heeger chain with one pair of PT-symmetric defects, Sci. Rep. **7**, 5903 (2017).

[20] B. Midya, W. Walasik, N. M. Litchinitser, and L. Feng, Supercharge optical arrays, arXiv: 1809.05756

[21] A. Blanco-Redondo, I. Andonegui, et al., Topological Optical Waveguiding in Silicon and the Transition between Topological and Trivial Defect States, Phys. Rev. Lett., **116**, 163901 (2016).

[22] I.S. Sinev, I.S. Mukhin, A. P. Slobozhanyuk, A. N. Poddubny, A. E. Miroshnichenko, A. K. Samuseva and Y. S. Kivshara, Mapping plasmonic topological states at the nanoscale, Nanoscale **7**, 11904 (2015).

[23] E. J. Meier, F. A. An and B. Gadway, Observation of the topological soliton state in the SuSchriefferHeeger model, Nature Commun. 13986 (2016).

[24] P. St-Jean, V. Goblot, E. Galopin, A. Lematre, T. Ozawa, L. Le Gratiet, I. Sagnes, J. Bloch and A. Amo, Lasing in topological edge states of a one-dimensional lattice, Nature Photonics 11, 651 (2017).

[25] H. Zhao, P. Miao, M. H. Teimourpour, S. Malzard, R. El-Ganainy, H. Schomerus and L. Feng, Topological hybrid silicon microlasers, Nature Commun. **9**, 981 (2018).

[26] M. Parto, S. Wittek et. al., Edge-Mode Lasing in 1D Topological Active Arrays, Phys. Rev. Lett. 120, 113901 (2018).

[27] M. Pan, H. Zhao, P. Miao, S. Longhi and L. Feng, Photonic zero mode in a non-Hermitian photonic lattice, Nature Communications **9**, 1308 (2018).

[28] J. Zak, Berrys phase for energy bands in solids, Phys. Rev. Lett. 62, 2747 (1989).

[29] J. Zak, Band Center-A Conserved Quantity in Solids, Phys. Rev. Lett **48**, 359 (1982).

[30] G. Miert, C. Ortix and C. M. Smith, Topological origin of edge states in two-dimensional inversion-symmetric insulators and semi metals, 2D Materials **4**, 015023 (2016).

[31] R. Morandotti, U. Peschel, J. S. Aitchison, H. S. Eisenberg and Y. Silberberg, Experimental Observation of Linear and Nonlinear Optical Bloch Oscillations, Phys. Rev. Lett. **83** 4756 (1999).

[32] T. Pertsch, P. Dannberg, W. Elflein, and A. Bräuer, and F. Lederer, Optical Bloch Oscillations in Temperature Tuned Waveguide Arrays, Phys. Rev. Lett. **83**, 4752 (1999).

[33] F. Grusdt, M. Honing, and M. Fleischhauer, Topological edge states in the one-dimensional superlattice Bose-Hubbard model, Phys. Rev. Lett. 110, 260405 (2013).

[34] R. Fleury, A. B. Khanikaev and A, Alu, Floquet topological insulators for sound, Nature Communications 7, 11744 (2016).

[35] N. Lang and H. Peter Büchler, Topological networks for quantum communication between distant qubits, npj Quantum Information 3, 47 (2017).

[36] S. Ryu and Y. Hatsugai, Topological Origin of Zero-Energy Edge States in Particle-Hole Symmetric Systems, Phys. Rev. Lett. **89**, 077002 (2002).

[37] S. Longhi, Quantum-optical analogies using photonic structures, Laser & Photonics Rev. **3**, 243 (2009).

[38] A. Szameit and S. Nolte, Discrete optics in femtosecond-laserwritten photonic structure, J. Phys. B: At. Mol. Opt. Phys. **43**, 163001 (2010).

[39] J.S. Aitchison, A.M. Weiner, Y. Silberberg, D.E. Leaird, M.K. Oliver, J.L. Jackel, and P.W.E. Smith, Experimental observation of spatial soliton interactions, Opt. Let. **16**, 15 (1991).